Photoinduced Intramolecular Electron Transfer in Conjugated Perylene Bisimide-Dithienothiophene Systems: A Comparative Study of a Small Molecule and a Polymer

Jie Huang,[†] Yishi Wu,[†] Hongbing Fu,*[,†] Xiaowei Zhan,*[,†] Jiannian Yao,*[,†] Stephen Barlow,[‡] and Seth R. Marder*[,‡]

Beijing National Laboratory for Molecular Sciences (BNLMS) and Institute of Chemistry, Chinese Academy of Sciences, Beijing 100190, People's Republic of China, and School of Chemistry and Biochemistry and Center for Organic Photonics and Electronics, Georgia Institute of Technology, Atlanta, Georgia 30332

Received: December 8, 2008; Revised Manuscript Received: February 23, 2009

The solution photophysical properties of two conjugated dithienothiophene (DTT)-perylene bisimide (PBI) systems—a polymer, poly{[*N,N*′-bis(2-decyl-tetradecyl)-3,4,9,10-perylene diimide-1,7-diyl]-*alt*-(dithieno[3,2-*b*:2′,3′-*d*]thiophene-2,6-diyl)}, and a small molecule, 1,7-bis(dithieno[3,2-*b*:2′,3′-*d*]thiophene-2-yl)-*N,N*′-bis(2-decyl-tetradecyl)-3,4,9,10-perylene diimide—in solution have been investigated. Strong quenching of the fluorescence of the PBI moiety was observed in both DTT-PBI systems, suggesting the possibility of an efficient intramolecular electron-transfer process. The kinetics of photoinduced electron transfer in the DTT-PBI polymer and monomer in solutions were explored by femtosecond time-resolved transient absorption spectra. It was found that both the rates of charge separation and charge recombination in the DTT-PBI polymer were approximately double those in the small molecule. This indicates that electronic coupling plays an important role in the electron-transfer process in a polymer system.

Introduction

Conjugated polymers are important materials for the fabrication of lightweight, low-cost, and large-area flexible ultrathin optoelectronic devices because of their optical and electrical properties combined with the possibility of tuning these properties through modulation of their molecular structures and their ease of processing.[1−6] Since the discovery of photoinduced electron transfer in composites of conducting polymers and fullerene, an increasing number of polymers that incorporated electron donor and/or electron acceptor moieties have been reported.[7−11] These donor−acceptor systems are constructed to enable energy and electron transfer after excitation with light, aiming at developing novel optoelectronic properties for applications in fields such as organic light-emitting diodes and organic solar cells.[12−15]

Especially in polymer solar cells, the efficiency of converting absorbed photons into charges as well as the subsequent transportation of these charges to the electrodes is strongly dependent on the degree of mesoscopic ordering of donor and acceptor moieties. In this context, covalently linked structures, such as diblock polymers, copolymers, and double-cable polymers, have been utilized to form a continuous network to realize a higher degree of mesoscopic ordering and/or a lower degree of phase separation and clustering at the molecular scale.[16−19] Although the synthesis and performance of these polymers incorporated in photovoltaic devices have been extensively investigated, their photophysical properties have not been fully explored and understood on short timescales.

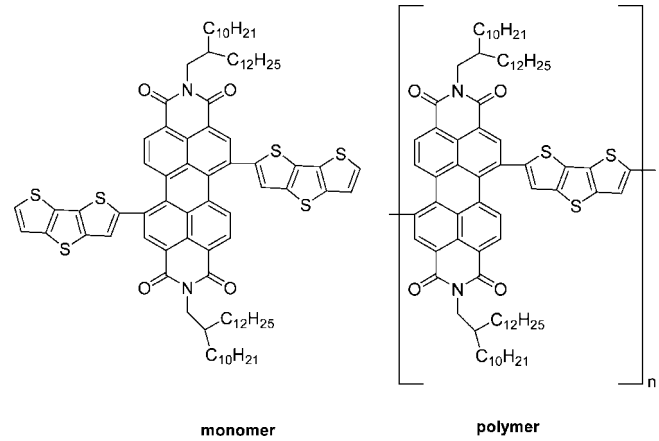

Figure 1. Structures of DTT-PBI monomer and polymer.

Perylene bisimide (PBI) dyes are among the most promising molecular building blocks with photonic and electronic functionality.[20] We have recently reported the properties of donor−acceptor copolymers, based on alternating dithienothiophene (DTT) and perylene bisimide (PBI) units, which exhibited high electron mobility and afforded very good photovoltaic performance, in bulk heterojunction devices in combination with polythiophene-based donors.[21] To gain further insight into the photophysical processes in DTT-PBI materials and to investigate the possibility of photocharge generation within these materials, we report here on the use of femtosecond transient absorption spectroscopy to probe the photoinduced electron-transfer process in the DTT-PBI polymer and in a small-molecule model (Figure 1).

Experimental Section

Steady-State Spectra Measurements. The steady-state absorption spectra were measured on a Perkin-Elmer lambda

* To whom correspondence should be addressed. Phone: +86-10-8261-6517; Fax: +86-10-8261-6517; E-mail: (H.F.) hongbing.fu@iccas.ac.cn, (X.Z.) xwzhan@iccas.ac.cn, (J.Y.) jnyao@iccas.ac.cn, (S.R.M.) seth.marder@chemistry.gatech.edu.
† Chinese Academy of Sciences.
‡ Georgia Institute of Technology.

10.1021/jp8107655 CCC: $40.75 © 2009 American Chemical Society
Published on Web 03/30/2009

35 spectrometer with a scanning speed of 480 nm/min and a slit width of 1 nm. The steady-state fluorescence spectra were acquired on a Hitachi F-4500 fluorescence spectrophotometer using a right angle configuration. Slits were set to provide widths of 5 nm for both the excitation and the emission monochromators. Sample solutions were examined in rectangular quartz cuvettes with a 1 cm path length. The fluorescence quantum yields were determined with dilute solutions ($A < 0.10$) by the comparative method using cresyl violet perchlorate as a standard (0.53 in methanol).[22] All measurements were carried out at room temperature. Solvents for all measurements were of the highest grade commercially available (Sigma-Aldrich) and used as received.

Quantum Chemical Calculations. The optimized structures and electron densities of the highest occupied molecular orbital (HOMO) and the lowest unoccupied molecular orbital (LUMO) of the DTT-PBI monomer and polymer were calculated by the Gaussian 03 suite of programs,[23] by using the density functional theory with the B3LYP/6-31G method.

Femtosecond Transient Absorption Measurements. A Ti−sapphire femtosecond laser system provided laser pulses for the femtosecond transient absorption measurements by using the pump-probe technique, as described in detail in our previous paper.[24] A regenerative amplifier (Spectra Physics, Spitifire) seeded with a mode-locked Ti−sapphire laser (Spectra Physics, Tsunami) delivered laser pulses at 800 nm (120 fs, 1 kHz), which were then divided into two components by using a beam splitter. The major component was sent to an optical parametric amplifier (Spectra Physics, OPA-800C) generating the pump pulses (620 nm, 130 fs, 1 kHz). The white-light continuum, generated by focusing the minor component into a sapphire plate, was then divided into a probe beam and a reference beam. The probe beam was overlapped with the pump beam at the sample. The reference beam was used to eliminate the influence of the laser beam fluctuations and subsequently enhance the signal-to-noise ratio. The optical delay times between the pump and probe beams were realized through a computer-controlled motorized translation stage. A magic-angle (54.7°) scheme was used in the pump-probe measurement to cancel out the orientation effects on the measured dynamics. The cross correlation function between the pump and probe pulses were determined to be about 150 fs full width at half-maximum (fwhm) by taking advantage of the technique based on the nonresonant optical Kerr effect. The transmitted light was detected by a liquid-nitrogen cooled CCD (Spectrum One, CCD-3000). The samples were irradiated at 620 nm with 0.2−1.0 μJ per pulse. The typical optical density of the sample at the excitation wavelength is 0.2−0.6 per mm. Steady-state absorption spectra were carried out before and after the transient absorption measurements to confirm that there was no photodegradation of the samples. Analysis of the kinetic data was performed both individually and globally using a nonlinear least-squares fit to a general sum-of-exponentials function with convolution of a Gaussian instrument response function of 150 fs fwhm. In the power-dependent experiments, all samples were excited by a laser pulse (400 nm, 130 fs), which was produced by the second harmonic generation (SHG) of the fundamental lasers (800 nm, 120 fs) by using a BBO crystal. The laser power was attenuated by a neutral density filter.

Results and Discussion

Synthesis and Molecular Structural Modeling. The synthesis and structural characterization of the DTT-PBI polymer, poly{[*N,N*′-bis(2-decyl-tetradecyl)-3,4,9,10-perylene diimide-1,7-diyl]-*alt*-(dithieno[3,2-*b*:2′,3′-*d*]thiophene-2,6-diyl)}, have been described previously.[21] The weight-average molecular weight (M_w) of the polymer was estimated to be 15 000 g/mol with a polydispersity index of 1.5, from size exclusion chromatography (SEC) against polystyrene standards on a PL-GPC model 210 chromatograph at 35 °C. The number-average degree of polymerization was thus accordingly estimated to be approximately 8. The synthesis and characterization of the small-molecule model, 1,7-bis(dithieno[3,2-*b*:2′,3′-*d*]thiophene-2-yl)-*N,N*′-bis(2-decyl-tetradecyl)-3,4,9,10-perylene diimide, will be published separately elsewhere.

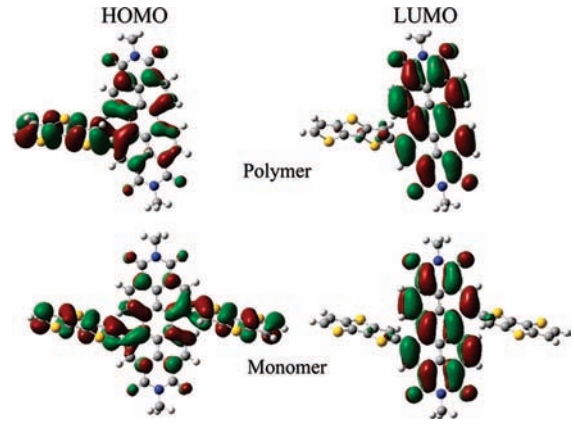

Figure 2. Optimized structures and the HOMOs (left) and LUMOs (right) of a single repeat unit of the DTT-PBI polymer (top) and small molecule (bottom) obtained by the density function method at the B3LYP/6-31G level. The long alkyl chains were replaced by methyl groups for simplicity during the optimizations and calculations.

In order to get preliminary insights into the electronic structures and interactions in the DTT-PBI polymer and the model compound, computational studies were performed by the density functional method at the B3LYP/6-31G level. Figure 2 shows the optimized structures and the HOMO and LUMO of the two systems. According to the calculations, the bay-substitutions introduced a twisting of the two naphthalene subunits in the perylene core by 7.1° for a single repeat unit of the polymer and 5.0° for the small molecule analogue. Moreover, the dihedral angles between the PBI moiety and the DTT moiety in these systems were determined to be 65.6° for a single repeat unit of the polymer and 55.9° for the small molecule analogue. These results indicated that reduced planarity and rigidity of the perylene cores were present in both systems. Similar results have also been found in other bay-substituted PBI dyes.[20,24,25] The molecular orbital (MO) diagrams are also very similar, indicating similar electron distribution in the two systems. The HOMOs are delocalized over both DTT and PBI moieties and can be regarded as out-of-phase combinations of the local DTT and PBI HOMOs, while the LUMOs are very similar to those of the unsubstituted PBI moiety.

Electrochemistry. The oxidation and reduction potentials of the DTT-PBI polymer film and small molecule solution were determined by cyclic voltammetry in Bu_4NPF_6−CH_3CN (vs ferrocene), as shown in Figure 3 and Table 1. One oxidation wave was observed in the cyclic voltammogram of the small molecule at a half-wave potential of $E_{ox1} = 0.84$ V, while one oxidation wave was found for the polymer at a peak potential of $E_{ox1} = 1.18$ V. The DTT-PBI polymer and small molecule exhibited almost the same two reduction potentials approximately at half-wave potentials of $E_{red1} = -1.0$ V and $E_{red2} = -1.2$ V. The oxidation seen for the small molecule can be attributed to oxidation of the molecule itself. Thiophene

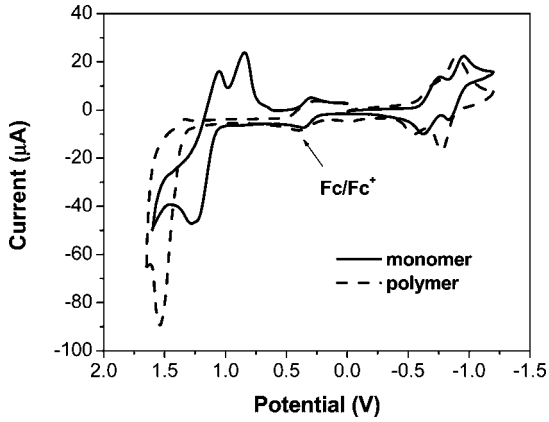

Figure 3. Cyclic voltammograms for the small molecule in solution and polymer film in CH_3CN/0.1 M $[^nBu_4N]^+[PF_6]^-$ with ferrocenium/ferrocene as an internal standard, at 50 mV/s.

TABLE 1: Redox Potentials of the DTT-PBI Polymer and Small Molecule (V vs Ferrocene)[a]

	polymer[a]	small molecule[b]
E_{ox1}[c]	1.18	0.84
E_{red1}[d]	−0.97	−1.02
E_{red2}[d]	−1.19	−1.22

[a] Film in CH_3CN/0.1 M $[^nBu_4N]^+[PF_6]^-$ versus ferrocenium/ferrocene at 50 mV s^{-1}. [b] Solution in CH_2Cl_2/0.1 M $[^nBu_4N]^+[PF_6]^-$ versus ferrocenium/ferrocene at 50 mV s^{-1}. [c] Peak potentials. [d] Half-wave potentials.

derivatives with α-H atoms have been extensively reported to be easily oxidized and therefore further oligomerized and/or polymerized.[26] The feature characterized by a peak potential of 0.51 V in the reduction scan can be attributed to a dimerization or oligomerization product formed from the oxidized molecule.

Steady-State Absorption and Fluorescence Spectra. The steady-state absorption spectra of the DTT-PBI monomer and polymer in $CHCl_3$ are shown in Figure 4a. In contrast, the unsubstituted PBIs, both small molecule and polymer, exhibit two bands within the visible/near-IR with the low-energy band (at 550−750 nm) being broad and more-or-less featureless, while the higher energy band (at 400−500 nm) retains some vibronic structure, at least in the small molecule. The features of the low-energy band, together with support by the calculations discussed above that show that the HOMO is largely localized on the DTT groups and the LUMO on the PBI groups, suggest a transition with considerable charge redistribution from the DTT units to the PBI core. The insensitivity of both absorption and emission spectra to solvent polarity indicate no dipolar charge-transfer character to these transitions, suggesting that the charge redistribution occurs in a quadrupolar fashion in both the small molecule and the polymer (see the Supporting Information). The retention of some vibronic structure in the higher-energy band may indicate a PBI-centered transition (with the loss of structure relative to an unsubstituted PBI being potentially attributable to the twisting of the core from planarity, as suggested by the calculations). A third band in the UV may be attributable to DTT-centered transitions. These spectra are qualitatively similar to those of the other 1,7-disubstituted PBIs with electron-rich substituents including oligothienyls,[27a] *p*-(diphenylamino)phenyl,[27b] and 4′-(diarylamino)-biphen-4-ylethynyl,[27c] while 1,7-disubstituted PBIs substituted with weaker donors such as *p*-(alkoxy)phenyl and *p*-alkoxyphenylethynyl,[27b] in which both the HOMO and LUMO are largely localized on the PDI core, typically exhibit one strong visible transition red-shifted from the parent PBI often retaining some vibronic structure. Compared with the small molecule, the maxima of both absorption bands of the polymer are red-shifted due to the increase in conjugation length. However, the extent of the red-shift is rather limited, suggesting that the effective conjugation length in the polymer was not large. This is consistent with the large twist angles calculated between the DTT and PBI units limiting effective long-range conjugation (vida supra).

Figure 4b shows the fluorescence spectra of the DTT-PBI polymer and monomer upon excitation of the PBI moieties in $CHCl_3$. As with the low-energy absorption band, the emission spectra are broad and exhibit reduced vibronic fine structure relative to unsubstituted PBIs. As with the absorption spectra, the polymer spectrum is only a little red-shifted compared to that of the small molecule, suggesting a low effective conjugation length in the polymer. However, the relative intensities between the 0−0 and 0−1 subbands are different, the 0−0 subband for monomer and 0−1 for polymer, respectively. Moreover, the spacing between the two sub-bands is larger in the monomer than that in the polymer.[28]

The fluorescence quantum yields of unsubstituted PBI dyes in different solvents have been reported to be close to unity, independent of solvent polarity.[20] However, much lower fluorescence quantum yields are observed on photoexcitation of the DTT-PBI polymer and small molecule in solution, as shown in Table 2, suggesting that channels for efficient nonradiative decays are present both in the polymer and small molecule. Moreover, the quantum yields decrease with increasing solvent polarity and are lower for the polymer than the small molecule. As can be seen from the absorption spectra in Figure 3a, the energy level of the singlet excited state of the DTT moiety is much higher than that of the PBI moiety in these systems, which excludes the energy transfer from the DTT to the PBI moiety upon excitation of the PBI moiety. This assumes that the low-energy band is purely PBI-centered, whereas orbitals and comparison to other compounds[27] suggests it has quadrupolar DTT→PBI character. One factor contributing to this fluorescence quenching in the DTT-PBI polymer and small molecule may be from an intramolecular electron-transfer process giving a charge-separated species; this has been observed in several other donor-substituted PBI systems[27] and is further supported by transient absorption spectra (vide infra).

Femtosecond Transient Absorption Spectra. The possibility of assigning the fluorescence quenching in these species to formation of a charge-separated state as a result of electron transfer were further directly confirmed by the solution femtosecond transient absorption spectra in the visible region.

DTT-PBI Small Molecule. When the DTT-PBI small molecule was excited at 620 nm with a 130 fs laser pulse in $CHCl_3$, the femtosecond transient absorption spectra yielded two positive absorption bands, with one centered at approximately 490 nm and the other centered at approximately 730 nm, as shown in Figure 5. The band centered at approximately 730 nm was attributed to the characteristic absorption of the $PBI^{\bullet-}$ radical anion,[24,29−32] further suggesting that a charge-separated state is indeed produced from the excited state of the DTT-PBI small molecule. Further analysis of the time profile of the absorption at 730 nm revealed that a fast rise and a slow decay component were involved with a time constant of 0.54 and 786 ps, respectively, as shown in Figure 6. The fast rise was attributed to the charge separation (CS) process, while the subsequent decay was ascribed to the charge recombination (CR) process. The rate constants of charge separation (k_{CS}) and charge

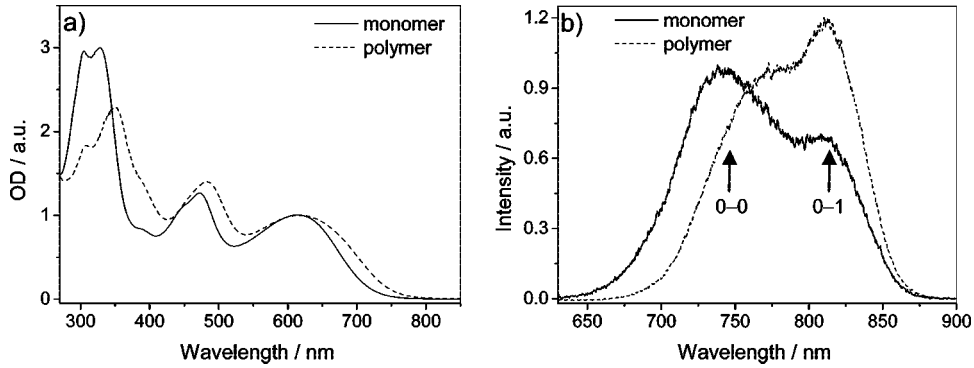

Figure 4. Normalized steady-state (a) absorption spectra and (b) emission spectra of the DTT-PBI polymer and monomer in $CHCl_3$. All the concentrations are 2×10^{-5} mol/L, $\lambda_{ex} = 620$ nm.

TABLE 2: Fluorescence Quantum Yields of DTT-PBI Polymer and Monomer in Different Solvents ($\lambda_{ex} = 620$ nm)

	polymer	small molecule
$CHCl_3$ ($\varepsilon = 4.9$)	0.0096	0.021
CH_2Cl_2 ($\varepsilon = 9.14$)	0.0047	0.013
EtOH ($\varepsilon = 25.7$)	0.00074	0.00082
CH_3OH ($\varepsilon = 32.7$)	0.00041	0.00047
DMSO ($\varepsilon = 45$)	$\sim 10^{-5}$	$\sim 10^{-5}$

recombination (k_{CR}) in $CHCl_3$ were thus accordingly determined as 1.9×10^{12} and 1.3×10^{9} s^{-1}, respectively. This rapid charge separation process is consistent with the almost complete quenching of the PBI emission. The detailed temporal evolution at 490 nm was identical with that at 730 nm, suggesting that this absorption might arise from a corresponding radical cation species, which would be expected to be principally localized on the DTT units. The unsubstituted $DTT^{\bullet+}$ radical cation has previously been shown to absorb at 411 nm (with another feature at 595 nm) in a freon matrix at 77 K,[33] and it is possible that this feature is red-shifted by extension of conjugation by the attached PBI unit in the present compound.

The transient absorption data in the entire $PBI^{\bullet-}$ radical anion absorption band between 650 and 750 nm were further globally analyzed, as shown in Figure 7a. The 0.54-ps time component showed a negative amplitude, suggesting the CS process, while the component of 786 ps displayed a positive amplitude, indicating the CR process. These results were consistent with those of the individual analysis above. The rates of both CS and CR in $CHCl_3$ are slower than those observed in CH_2Cl_2 (Table 3).

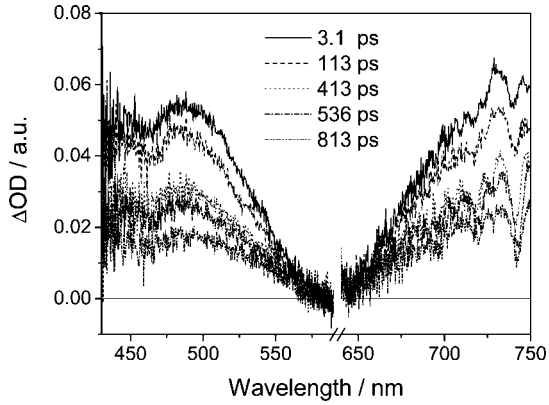

Figure 5. Femtosecond transient absorption spectra of the DTT-PBI monomer in $CHCl_3$ upon excitation at 620 nm with a 130 fs laser pulse in different delay times as indicated in the spectra. The spectra near 620 nm due to laser scattering were deleted for clarity.

The free energy changes ($-\Delta G$) of the radical ion pairs, charge separation ($-\Delta G_{CS}$), and charge recombination ($-\Delta G_{CR}$) were estimated using eqs 1−3.[34]

$$\Delta G = e[E_{ox}(D) - E_{red}(A)] - \frac{e^2}{\varepsilon_s r_{DA}} - \frac{e^2}{2}\left(\frac{1}{r_D} + \frac{1}{r_A}\right)\left(\frac{1}{\varepsilon_p} + \frac{1}{\varepsilon_s}\right) \quad (1)$$

$$\Delta G_{CS} = \Delta G - E_{00} \quad (2)$$

$$\Delta G_{CR} = -\Delta G \quad (3)$$

The first oxidation potential of the donor (i.e., the DTT moiety, $E_{ox}(D)$) and the first reduction potential of the acceptor (i.e., the PBI moiety, $E_{red}(A)$) were taken from the cyclic voltammetry measurements in MeCN ($\varepsilon_s = 36.6$) described above. The radius of the DTT radical cation r_D was approximately estimated to be 3.64 Å from the X-ray crystallographic data of unsubstituted DTT.[35] The radius of the PBI radical anion r_A was estimated to be 4.71 Å based on the X-ray crystallographic data of *N*,*N*′-dimethylperylene-3,4:9,10-tetracarboxylic-bisimide.[36] (Wasielewski has suggested somewhat larger radii are necessary to correctly model PBIs and their associated solvation.[37]) r_{DA} was taken to be the distance between the centers of the PBI and DTT moieties; a value of 7.17 Å was obtained from the structure optimized by a molecular modeling at the B3LYP/6-31G level. E_{00} is the energy of the relaxed lowest excited singlet state of the system and was taken as 2.00 eV in $CHCl_3$ ($\varepsilon_s = 4.9$). The estimated free energy changes of photoexcited charge separation (ΔG_{CS}) and charge recombination (ΔG_{CR}) in these dyads are listed in Table 3 and suggest that these processes are exergonic in both $CHCl_3$ and CH_2Cl_2. The driving force estimated for charge separation ($-\Delta G_{CS}$) is larger in CH_2Cl_2, while that for charge recombination (ΔG_{CR}) is larger in $CHCl_3$. Accordingly, the observation that the rates of charge separation and recombination are both higher in CH_2Cl_2 suggests that the charge separation process is in the normal Marcus region, while charge recombination is in the inverted region.[38] This is in line with several other studies of intramolecular charge separation and recombination with driving forces of comparable orders of magnitude.[39] However, this analysis should be treated with caution; the estimate of the driving force assumes charge separation from an excited state localized on one of the two components, whereas the orbitals shown in Figure 2 and the absorption spectra are consistent with

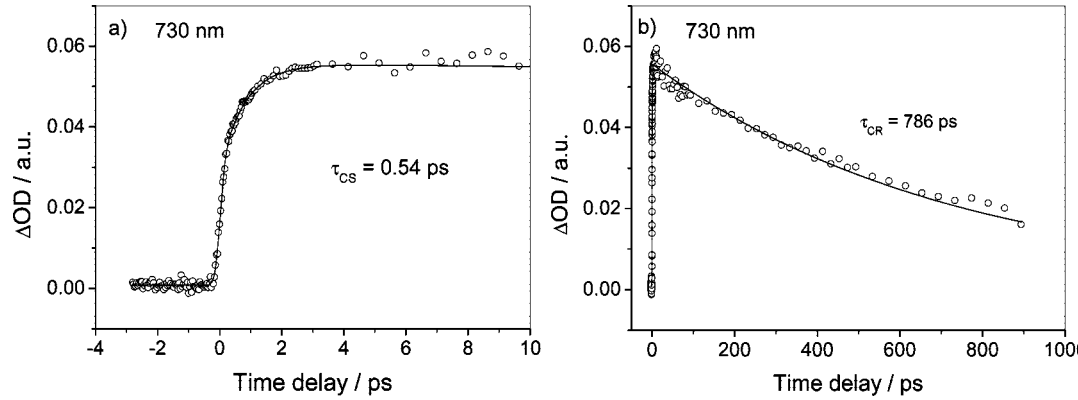

Figure 6. Time profiles of the transient absorption at 730 nm at (a) short and (b) long time windows. Fits are also shown as solid lines.

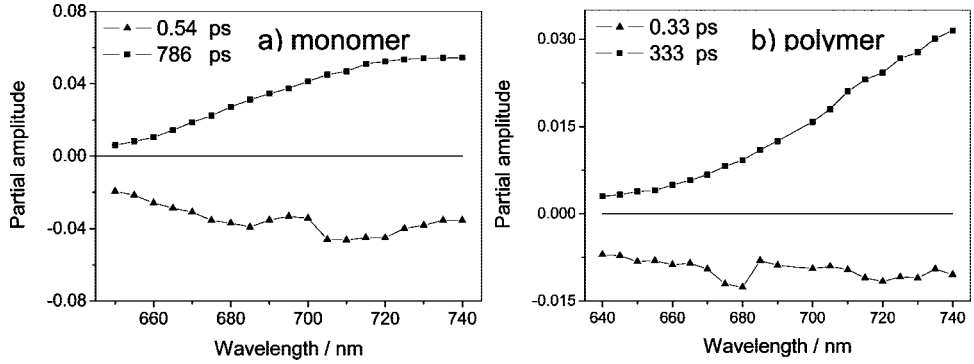

Figure 7. Wavelength dependence of the partial amplitudes of the decay times obtained by global analysis of the femtosecond transient absorption of the DTT-PBI monomer (a) and polymer (b) in $CHCl_3$.

TABLE 3: Charge Separation and Charge Recombination Data for the DTT-PBI Polymer and Small Molecule in Different Solvents

	polymer					small molecule				
	ΔG_{CS} [eV]	ΔG_{CR} [eV]	λ_s [eV]	τ_{CS} [ps]	τ_{CR} [ps]	ΔG_{CS} [eV]	ΔG_{CR} [eV]	λ_s [eV]	τ_{CS} [ps]	τ_{CR} [ps]
$CHCl_3$ (ε = 4.9)	−0.04	−1.96	0.40	1.71	867	−0.33	−1.67	0.40	2.65	1462
CH_2Cl_2 (ε = 9.14)	−0.18	−1.82	0.52	0.33	333	−0.47	−1.53	0.52	0.54	786

some quadrupolar charge separation in the excited state, prior to the "charge separation" process observed in the transient spectra.

DTT-PBI Polymer. The femtosecond transient absorption spectra of DTT-PBI polymer in $CHCl_3$ showed a very similar pattern with that of the small molecule when the polymer was excited at 620 nm with a 130 fs laser pulse, as shown in Figure 8. As in the small molecule, the band centered at approximately 730 nm was attributed to the characteristic absorption of the $PBI^{\bullet-}$ radical anion; the fast rise and slow decay were characterized by time constants of 0.33 and 333 ps, respectively, as shown in Figure 9, giving rate constants of charge separation (k_{CS}) and charge recombination (k_{CR}) in $CHCl_3$ of 3.0×10^{12} and 3.0×10^9 s^{-1}, respectively. The more rapid charge separation in the polymer, compared to that in the small molecule, is consistent with the stronger fluorescence quenching in the former system. The detailed temporal evolution at 530 nm was revealed to be identical with that at 730 nm; therefore, the band centered at 530 nm might be due to the absorption of a radical cation species. However, it should be noted that this peak in the polymer is considerably red-shifted as compared with that assigned to $DTT^{\bullet+}$ in the small molecule or reported for unsubstituted $DTT^{\bullet+}$. This perhaps suggests a cation probably delocalized over a few units of the polymer rather than being localized on one or two of the $DTT^{\bullet+}$ units in the small molecule.

The transient absorption data in the entire $PBI^{\bullet-}$ radical anion absorption band between 650 and 750 nm were further globally analyzed, as shown in Figure 7b. The 0.33-ps time component showed a negative amplitude, suggesting the charge separation (CS) process, while the component of 333 ps displayed a positive amplitude, indicating the charge recombination (CR)

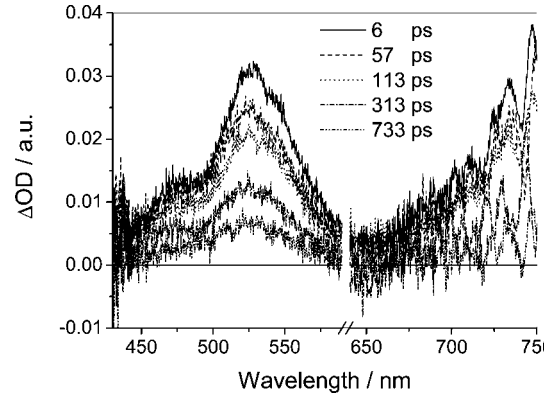

Figure 8. Femtosecond transient absorption spectra of the DTT-PBI polymer in $CHCl_3$ upon excitation at 620 nm with a 130 fs laser pulse in different delay times as indicated in the spectra. The portions of the spectra near 620 nm, which are affected by laser scattering, were deleted for clarity.

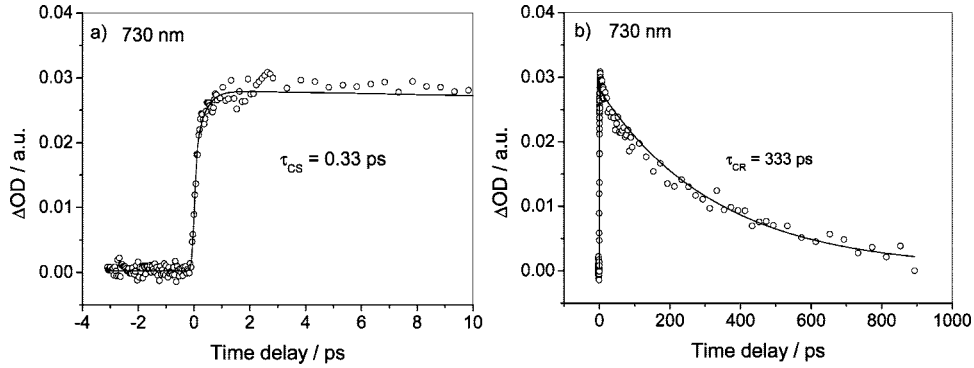

Figure 9. Time profiles of the transient absorption at 730 nm at (a) short and (b) long time windows. Fits are also shown in solid lines.

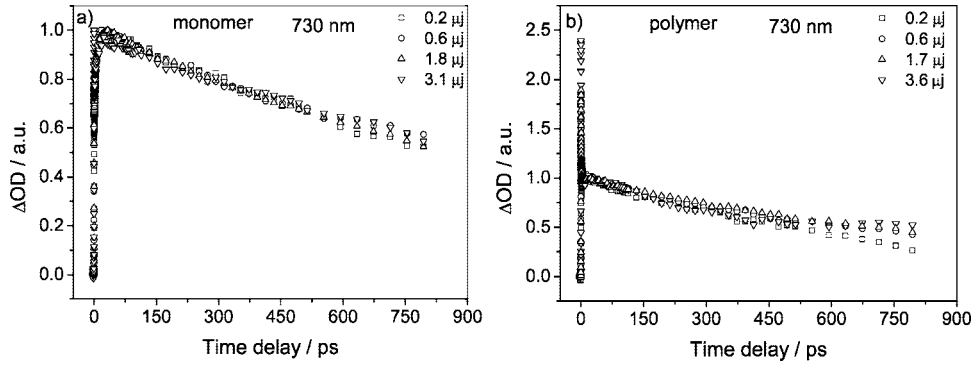

Figure 10. Power-dependent decays of the transient absorption at 730 nm of DTT-PBI (a) monomer and (b) polymer upon excitation at 400 nm with a 130 fs laser pulse in $CHCl_3$. The decays were normalized to facilitate comparison.

process. These results were consistent with those of individual analysis above.

As in the case of the small molecule, the time constants for charge separation and charge recombination in $CHCl_3$ are slower than those observed in CH_2Cl_2 (Table 3), with comparison with driving forces (Table 3, estimated in the same way as for the monomer, with the same values of E_{00}, r_A, r_D, and r_{DA}) again suggesting that charge separation and recombination processes occur in normal and inverted Marcus regions, respectively.

In a given solvent, the estimated driving force for charge separation ($-\Delta G_{CS}$) in the small molecule was about 0.6 eV higher than that of the polymer, while that for charge recombination ($-\Delta G_{CS}$) is approximately 0.6 eV lower. If the charge separation and recombination processes are indeed in the normal and inverted Marcus regimes, respectively, as suggested by the solvent-dependent study and the method used to estimate driving forces is applicable, then these differences in driving forces between the small molecule and the polymer are apparently at variance with the shorter time constants obtained for CS and CR processes in the polymer.

One possible explanation for the faster dynamics in the polymer might lie in biphoton and multiphoton processes that have been reported to play a role when conjugated polymers and some densely packed small molecules are excited at high excitation intensity. These processes are reported to lead to an increased rate of exciton quenching with the increase in excitation intensity as a result of exciton annihilation.[40] In order to examine whether the exciton annihilation process was present in our systems, we carried out power-dependent experiments; the results are shown in Figure 10. It can be seen that laser intensity has little effect on the decay rates of the polymer and the small molecule. Therefore, under the conditions of our experiments, biphoton and multiphoton processes play no significant role and cannot explain the faster dynamics in the polymer.

Thus, the faster dynamics in the polymer are presumably due to differences in donor−acceptor electronic coupling and/or reorganization energy or, if the electronic coupling in these systems is sufficiently strong that that the electron-transfer reactions are adiabatic, to differences in the vibronic modes within these systems. However, distinguishing between these possibilities is beyond the scope of the current work.

Finally, we consider the implications of this study for the use of polymers of this type in photovoltaic applications. The rate constants for charge recombination are much slower than those for charge separation both in the DTT-PBI polymer and monomer ($k_{CS}/k_{CR} > 1000$). However, it should be noted that there will be a barrier to dissociation of the intramolecular charge-separated states we describe to give the free carriers desirable in a photovoltaic device due to the electrostatic interaction between cation and anion centers. This dissociation must occur within the relatively short lifetime of the charge-separated state. Indeed, it has recently been shown that, in films of 1,7-di(arylethynyl)perylene diimides, intramolecular charge separation hinders intermolecular charge separation, with the intramolecular charge-separated state serving to accelerate the decay of excited states to the ground state.[27c] Moreover, some of the holes and electrons generated in different parts of the DTT-PBI phase may anhilate one another en route to their respective electrodes. Thus, the photoinduced intramolecular charge separation in the polymer suggested by the present study may explain why the incident-photon-conversion-efficiency versus wavelength plot of a photovoltaic device based on a bulk heterojunction formed between the DTT-PBI polymer and a polythiophene derivative is close to the absorption spectrum of the polythiophene, with little contribution from the lower energy absorptions of the DTT-PBI material.[21a] In these devices, the main contribution to the photocurrent likely comes from relatively long-lived polythiophene excitons,[44,45] which diffuse to and dissociate at the polythiophene/DTT-PBI interface, with

the DTT-PBI polymer functioning principally as an electron-transport material.

Conclusions

In conclusion, we have investigated the properties of photo-induced electron transfer in conjugated dithienothiophene and perylene bisimide DTT-PBI polymer and monomer systems in solutions. Transient absorption spectra were recorded to demonstrate that both the rates of charge separation and charge recombination in the polymer were faster than those in the monomer, with these differences being perhaps attributable to stronger donor−acceptor coupling in the former system. Charge separation occurs on the time scale of 10^{-1} ps and is apparently taking place in the normal Marcus region, while the lifetimes of the charge separated states are in the range from 10^{-2} to 10^{-3} ps, with charge recombination apparently occurring in the Marcus inverted region. The intramolecular charge separation process in these materials may be related to the low contribution to the photocurrent made by the polymer in bulk heterojunction devices with a polythiophene derivative.

Acknowledgment. This work was supported by National Natural Science Foundation of China (Nos. 50221201, 90301010, 20373077, 20471062, 50573084, 90606004, 50873107, 20721061), the Chinese Academy of Sciences, the Ministry of Science and Technology of China (2006CB806200, 2006CB932100, 2006AA03Z220), the Sciece and Technology Center Program of the National Science Foundation (DMR-0120967), and the Office of Naval Research (through a MURI, N00014-03-1-0793, administered through the California Institute of Technology, and through N00014-04-1-0120).

Supporting Information Available: Steady-state absorption and emission spectra of DTT-PBI polymer and monomer in different solutions. This material is available free of charge via the Internet at http://pubs.acs.org.

References and Notes

(1) Burroughes, J. H.; Bradley, D. D. C.; Brown, A. R.; Marks, R. N.; Mackay, K.; Friend, R. H.; Burn, P. L.; Holmes, A. B. *Nature* **1990**, *347*, 539.

(2) Leni, A. *Prog. Polym. Sci.* **2003**, *28*, 875.

(3) *Organic Photovoltaics: Mechanisms, Materials, and Devices*; Sun, S. S., Sariciftci, N. S., Eds; CRC Press: Boca Raton, FL, 2005.

(4) Mozer, A. J.; Sariciftci, N. S. C. R. *Chimie* **2006**, *9*, 568.

(5) *Semiconducting Polymers: Chemistry, Physics and Engineering*, 2nd ed.; Hadziioannou, G., Malliaras, G. G., Eds; Wiley-VCH: Weinheim, Germany, 2006.

(6) Shirota, Y.; Kageyama, H. *Chem. Rev.* **2007**, *107*, 953.

(7) Sariciftci, N. S.; Smilowitz, L.; Heeger, A. J.; Wudl, F. *Science* **1992**, *258*, 1474.

(8) Morita, S.; Zakhidov, A. A.; Yoshino, K. *Solid State Commun.* **1992**, *82*, 249.

(9) Yang, X.; Loos, J.; Veenstra, S. C.; Verhees, W. J. H.; Wienk, M. M.; Kroon, J. M.; Michels, M. A. J.; Janssen, R. A. J. *Nano Lett.* **2005**, *5*, 579.

(10) Hou, J. H.; Tan, Z. A.; Yan, Y.; He, Y. J.; Yang, C. H.; Li, Y. F. *J. Am. Chem. Soc.* **2006**, *128*, 4911.

(11) Günes, S.; Neugebauer, H.; Sariciftci, N. S. *Chem. Rev.* **2007**, *107*, 1324.

(12) Peng, Q.; Park, K.; Lin, T.; Durstock, M.; Dai, L. *J. Phys. Chem. B* **2008**, *112*, 2801.

(13) Gómez, R.; Veldman, D.; Blanco, R.; Seoane, C.; Segura, J. J.; Janssen, R. A. J. *Macromolecules* **2007**, *40*, 2760.

(14) Galand, E. M.; Kim, Y.-G.; Mwaura, J. K.; Jones, A. G.; McCarley, T. D.; Shrotriya, V.; Yang, Y.; Reynolds, J. R. *Macromolecules* **2006**, *39*, 9132.

(15) Casalbore-Miceli, G.; Gallazzi, M. C.; Zecchin, S.; Camaioni, N.; Geri, A.; Bertarelli, C. *Adv. Funct. Mater.* **2003**, *13*, 307.

(16) Schmidt-Mende, L.; Fechtenkötter, A.; Müllen, K.; Moons, E.; Friend, R. H.; MacKenzie, J. D. *Science* **2001**, *293*, 1119.

(17) Peeters, E.; van Hal, P. A.; Meskers, S. C. J.; Janssen, R. A. J.; Meijer, E. W. *Chem. Eur. J.* **2002**, *8*, 4470.

(18) van Duren, J. K. J.; Yang, X. N.; Loos, J.; Bulle-Lieuwma, C. W. T.; Sieval, A. B.; Hummelen, J. C.; Janssen, R. A. J. *Adv. Funct. Mater.* **2004**, *14*, 425.

(19) Neuteboom, E. E.; Meskers, S. C. J.; van Hal, P. A.; van Duren, J. K. J.; Meijer, E. W.; Janssen, R. A. J.; Dupin, H.; Pourtois, G.; Cornil, J.; Lazzaroni, R.; Brédas, J.-L.; Beljonne, D. *J. Am. Chem. Soc.* **2003**, *125*, 8625.

(20) Würthner, F. *Chem. Commun.* **2004**, *14*, 1564.

(21) (a) Zhan, X. W.; Tan, Z. A.; Domercq, B.; An, Z. S.; Zhang, X.; Barlow, S.; Li, Y. F.; Zhu, D. B.; Kippelen, B.; Marder, S. R. *J. Am. Chem. Soc.* **2007**, *129*, 7246. (b) Tan, Z. A.; Zhou, E.; Zhan, X. W.; Wang, X.; Li, Y. F.; Barlow, S.; Marder, S. R. *Appl. Phys. Lett.* **2008**, *93*, 073309.

(22) Isak, S. J.; Eyring, E. M. *J. Phys. Chem.* **1992**, *96*, 1738.

(23) Frisch, M. J.; Trucks, G. W.; Schlegel, H. B.; Scuseria, G. E.; Robb, M. A.; Cheeseman, J. R.; Montgomery, J. A., Jr.; Vreven, T.; Kudin, K. N.; Burant, J. C.; Millam, J. M.; Iyengar, S. S.; Tomasi, J.; Barone, V.; Mennucci, B.; Cossi, M.; Scalmani, G.; Rega, N.; Petersson, G. A.; Nakatsuji, H.; Hada, M.; Ehara, M.; Toyota, K.; Fukuda, R.; Hasegawa, J.; Ishida, M.; Nakajima, T.; Honda, Y.; Kitao, O.; Nakai, H.; Klene, M.; Li, X.; Knox, J. E.; Hratchian, H. P.; Cross, J. B.; Adamo, C.; Jaramillo, J.; Gomperts, R.; Stratmann, R. E.; Yazyev, O.; Austin, A. J.; Cammi, R.; Pomelli, C.; Ochterski, J. W.; Ayala, P. Y.; Morokuma, K.; Voth, G. A.; Salvador, P.; Dannenberg, J. J.; Zakrzewski, V. G.; Dapprich, S.; Daniels, A. D.; Strain, M. C.; Farkas, O.; Malick, D. K.; Rabuck, A. D.; Raghavachari, K.; Foresman, J. B.; Ortiz, J. V.; Cui, Q.; Baboul, A. G.; Clifford, S.; Cioslowski, J.; Stefanov, B. B.; Liu, G.; Liashenko, A.; Piskorz, P.; Komaromi, I.; Martin, R. L.; Fox, D. J.; Keith, T.; Al-Laham, M. A.; Peng, C. Y.; Nanayakkara, A.; Challacombe, M.; Gill, P. M. W.; Johnson, B.; Chen, W.; Wong, M. W.; Gonzalez, C.; Pople, J. A. Gaussian 03, revision B.03; Gaussian, Inc.: Pittsburgh, PA, 2003.

(24) Huang, J.; Fu, H. B.; Wu, Y. S.; Chen, S. Y.; Shen, F. G.; Zhao, X. H.; Liu, Y. Q.; Yao, J. N. *J. Phys. Chem. C* **2008**, *112*, 2689.

(25) Wolcan, E.; Ferraudi, G. *J. Phys. Chem. A* **2000**, *104*, 9281.

(26) Hill, M. G.; Penneau, J.-F.; Zinger, B.; Mann, K. R.; Miller, L. L. *Chem. Mater.* **1992**, *4*, 1106.

(27) (a) Chen, S.; Liu, Y.; Qiu, W.; Sun, X.; Ma, Y.; Zhu, D. *Chem. Mater.* **2005**, *17*, 2208. (b) Chao, C.-C.; Leung, M.-k.; Su, Y. O.; Chiu, K.-Y.; Lin, T.-H.; Shieh, S.-J.; Lin, S.-C. *J. Org. Chem.* **2005**, *70*, 4323. (c) Shoaee, S.; Eng, M. P.; An, Z.; Zhang, X.; Barlow, S.; Marder, S. R.; Durrant, J. R. *Chem. Commun.* **2008**, 4915.

(28) Wang, W.; Wan, W.; Zhou, H. H.; Niu, S. Q.; Li, A. D. Q. *J. Am. Chem. Soc.* **2003**, *125*, 5248.

(29) Neuteboom, E. E.; Meskers, S. C. J.; Beckers, E. H. A.; Chopin, S.; Janssen, R. A. J. *J. Phys. Chem. A* **2006**, *110*, 12363.

(30) Ohkubo, K.; Kotani, H.; Shao, J.; Ou, Z. P.; Mkadish, K.; Li, G. L.; Pandey, R. K.; Fujitsuka, M.; Ito, O.; Imahori, H.; Fukuzumi, S. *Angew. Chem., Int. Ed.* **2004**, *43*, 853.

(31) Würthner, F.; Chen, Z. J.; Osswald, F. J. M. H. P.; You, C.-C.; Jonkheijm, P.; Herrikhuyzen, J. V.; Schenning, A. P. H. J.; van der Schoot, P. P. A. M.; Meijer, E. W.; Beckers, E. H. A.; Meskers, S. C. J.; Janssen, R. A. J. *J. Am. Chem. Soc.* **2004**, *126*, 10611.

(32) Kelley, R. F.; Tauber, M. J.; Wasielewski, M. R. *J. Am. Chem. Soc.* **2006**, *128*, 4779.

(33) Fujitsuka, M.; Sato, T.; Shimidzu, T.; Watanabe, A.; Ito, O. *J. Phys. Chem. A* **1997**, *101*, 1056.

(34) (a) Rehm, D.; Weller, A. A. *Isr. J. Chem.* **1970**, *8*, 259. (b) Weller, A. *Z. Phys. Chem. Neue Folge* **1982**, *133*, 93.

(35) Bertinelli, F.; Palmieri, P.; Stremmenos, C.; Pelizzi, G.; Taliani, C. *J. Phys. Chem.* **1983**, *87*, 2317.

(36) Hädicke, E.; Graser, F. *Acta Crystallogr., Sect. C: Cryst. Struct. Commun.* **1986**, *42*, 189.

(37) Lukas, A. S.; Zhao, Y.; Miller, S. E.; Wasielewski, M. R. *J. Phys. Chem. B* **2002**, *106*, 1299.

(38) (a) Marcus, R. A. *J. Chem. Phys.* **1956**, *24*, 979. (b) Marcus, R. A.; Sutin, N. *Biochim. Biophys. Acta* **1985**, *811*, 265.

(39) (a) Imahori, H.; Tamaki, K.; Guldi, D. M.; Luo, C.; Fujitsuka, M.; Ito, O.; Sakata, Y.; Fukuzumi, S. *J. Am. Chem. Soc.* **2001**, *123*, 2607. (b) Schuster, D. I.; Cheng, P.; Jarowski, P. D.; Guldi, D. M.; Luo, C.; Echegoyen, L.; Pyo, S.; Holzwarth, A. R.; Braslavsky, S. E.; Williams, R. M.; Klihm, G. *J. Am. Chem. Soc.* **2004**, *126*, 7257.

(40) (a) Scheblykin, I. G.; Yartsev, A.; Pullerits, T.; Gulbinas, V.; Sundström, V. *J. Phys. Chem. B* **2007**, *111*, 6303. (b) Fron, E.; Bell, T. D. M.; Van Vooren, A.; Schweitzer, G.; Cornil, J.; Beljonne, D.; Toele, P.; Jacob, J.; Müllen, K.; Hofkens, J.; Van der Auweraer, M.; De Schryver, F. C. *J. Am. Chem. Soc.* **2007**, *129*, 610. (c) Moll, J.; Harrison, W. J.; Brumbaugh, D. V.; Muenter, A. A. *J. Phys. Chem. A* **2000**, *104*, 8847.

(41) (a) Jortner, J. *J. Chem. Phys.* **1976**, *64*, 4860. (b) Marcus, R. A. *Angew. Chem., Int. Ed.* **1993**, *32*, 1111.

(42) Hutchison, G. R.; Ratner, M. A.; Marks, T. J. *J. Am. Chem. Soc.* **2005**, *127*, 2339.
(43) Li, W.-S.; Kim, K. S.; Jiang, D.-L.; Tanaka, H.; Kawai, T.; Kwon, J. H.; Kim, D.; Aida, T. *J. Am. Chem. Soc.* **2006**, *128*, 10527.
(44) Kraabel, B.; Moses, D.; Heeger, A. J. *J. Chem. Phys.* **1995**, *103*, 5102.
(45) van der Horst, J.-W.; Bobbert, P. A.; de Jong, P. H. L.; Michels, M. A.; Siebbeles, L. D. A.; Warman, J. M.; Gelinck, G. H.; Brocks, G. *Chem. Phys. Lett.* **2001**, *334*, 303.

JP8107655